Nanoscale

Novel layered Bi3MoMTO9 (MT = Mn, Fe, Co and Ni) thin films with tunable multifunctionalities

Journal:	*Nanoscale*
Manuscript ID	NR-ART-01-2020-000083.R1
Article Type:	Paper
Date Submitted by the Author:	18-Feb-2020
Complete List of Authors:	Gao, Xingyao; Purdue University, School of Materials Engineering Li, Leigang; Purdue University, School of Materials Engineering Zhang, Di; Purdue University, School of Materials Engineering Wang, Xuejing; Purdue University, School of Materials Engineering Jian, Jie; Purdue University, School of Materials Engineering He, Zihao; Purdue University, School of Electrical and Computer Engineering Wang, Haiyan; Purdue University System, MSE; Neil Armstrong Engineering Building

Novel layered $Bi_3MoM_TO_9$ (M_T = Mn, Fe, Co and Ni) thin films with tunable multifunctionalities

Xingyao Gao,[1] Leigang Li,[1] Di Zhang,[1] Xuejing Wang,[1] Jie Jian,[1] Zihao He,[2] and Haiyan Wang[1,2*]

[1]School of Materials Engineering, Purdue University, West Lafayette, IN 47907, United States

[2]School of Electrical and Computer Engineering, Purdue University, West Lafayette, IN 47907, United States

*To whom correspondence should be addressed: hwang00@purdue.edu

Abstract

$Bi_3MoM_TO_9$ ($BMoM_TO$; M_T, transition metals of Mn, Fe, Co and Ni) thin films with a layered supercell structure have been deposited on $LaAlO_3$ (001) substrates by pulsed laser deposition. Microstructural analysis suggests that the pillar-like domains with higher transition metal concentration (e.g., Mn, Fe, Co and Ni) are embedded in the Mo-rich matrix with layered supercell structures. The layered supercell structure of the $BMoM_TO$ thin films is accounted for the anisotropic multifunctionalities such as the magnetic easy axis along the in-plane direction, and the anisotropic optical properties. Ferroelectricity and ferromagnetism have been demonstrated in the thin films under room temperature, which confirms the multiferroic nature of the system. By varying the transition metal M_T in the film, the band gaps of the $BMoM_TO$ films can be effectively tuned from 2.44 eV to 2.82 eV, while the out-of-plane dielectric constant of the thin films also varies. The newly discovered layered nanocomposite systems presents their potentials in ferroelectrics, multiferroics and non-linear optics.

Introduction

Aurivillius phases, in perovskite-related structures with the formula of $Bi_2A_{n-1}B_nO_{3n+3}$ (A = Ca, Sr, Ba, Pb, Bi, Na, K, B = Ti, Nb, Ta, Mo, W, Fe),[1,2] have sparked significant research interests due to their potential applications in piezoelectric devices,[3–5] superconductors,[6–8] thermoelectric generators,[9,10] photocatalysts,[11,12] etc. In an Aurivillius lattice, n perovskite-like $(Bi_2A_{n-1}B_{3n+1})^{2-}$ layers and one bismuth-oxygen $(Bi_2O_2)^{2+}$ layer are stacked alternatively,[13] which generates an unique layered structure and promising properties. Due to the structural differences along the crystallographic orientations that are either parallel or perpendicular to the $(Bi_2O_2)^{2+}$ layers, anisotropic properties have been reported in many Aurivillius systems. For example, anisotropic optical property has been reported in the Bi_2AlMnO_6 supercell (SC) thin film;[14] anisotropic ionic conductivity has been demonstrated in $Bi_4V_{2-x}Co_xO_{11-\delta}$ single crystal;[15] and anisotropic dielectric constant has been observed in $BaBi_2Nb_2O_9$ system.[16] Besides, the Aurivillius phase has shown low leakage[17,18] and fatigue free[19,20] ferroelectric properties at the room temperature, which brings it potential applications in ferroelectric random access memories (FRAMs).[21]

Over the past few decades, considerable attention has been attracted on exploring multiferroic materials. Multiferroics are materials that simultaneously possess more than one ferroic characteristics (i.e. ferroelectricity, ferromagnetism and ferroelasticity),[22,23] which can be used in sensors, data storage, high-temperature electronics and memory devices.[24–26] The perovskite-type oxides with the formula of AM_TO_3 (A = Bi, P_b; M_T = transition metal ion) have been demonstrated as the candidates for the single phase multiferroic materials.[27] For example, $BiMnO_3$ has been reported as a multiferroic material which has the coexisting ferromagnetic and ferroelectric responses.[28,29] Beside of the single phase multiferroic materials, multiphase materials which combine different ferroic orders into one system have been well studied to artificially generate

multiferroic property.[30–32] Despite the tremendous efforts that have been spent on exploring new systems, single phase multiferroic materials are still rare in nature.

In this work, the layered Aurivillius phase Bi_2MoO_6 (BMoO) has been incorporated with the perovskite-type transition metal oxides BiM_TO_3 (BM_TO, M_T = Mn, Fe, Co and Ni) to form a new multiferroic nanocomposite system. BMoO is a ferroelectric material with a high Curie temperature (570 ^oC),[33] while BM_TO is a multiferroic system as mentioned above. Interestingly, by combining BMoO and BM_TO, a new nanocomposite material system ($Bi_3MoM_TO_9$, or $BMoM_TO$ as the abbreviation) has been created. Layered SC structure, which is similar to the Aurivillius phase, has been observed in this new material system. Meanwhile, pillar-like domains have been generated inside the thin films. Fig. 1(a) shows the 3D schematic drawing of the $BMoM_TO$ thin films, illustrating the pillar like domains embedded in layered matrix structure. The enlarged schematic illustration demonstrates that the crystal structure is consist of the alternatively stacked two Bi-O layers and one Mo/M_T-O layer. Besides, the $BMoM_TO$ thin films have exhibited tunable multifunctionalities, including room-temperature multiferroic properties (i.e. ferroelectricity and ferromagnetism) and optical properties (band gap and dielectric constant). These functionalities are anisotropic due to the layered structure and can be effectively tuned by changing the category of transition metal in the system.

Results and Discussion

X-ray diffraction (XRD) analysis was first conducted to characterize the microstructure and growth quality of the thin films. Fig. 1(b) shows the normalized θ-2θ XRD pattern of the $BMoM_TO$ thin films and pure BMoO thin film grown on $LaAlO_3$ (LAO) (001) substrates. From the XRD patterns, periodic (00*l*)-type diffraction peaks can be observed, indicating the high quality SC structure of the thin films with the preferential growth along out-of-plane (OP) direction.

Corresponding OP d-spacing of the thin films can be calculated by Bragg's law, while all the films have the similar lattice parameters of around 8.1 Å, as compared in Fig. S1. This result is predictable from the XRD patterns, where there is no obvious film peak shift for different films, indicating the similar SC structures in $BMoM_TO$ and BMoO thin films. The pure BMoO thin film has sharper peaks with a smaller full width at half maximum (FWHM), indicating higher crystallinity of the pure film comparing to the thin films. This result might be related to the formation of the domains in the film, which is to be discussed further below.

To better understand the microstructure of the $BMoM_TO$ thin films, cross-sectional transmittance electron microscopy (TEM)was conducted. Fig. 2(a) shows the cross-sectional TEM image of the Bi_3MoFeO_9 (BMoFeO) thin film grown on LAO (001) substrate. Overall, the film shows a layered SC structure with the lattice planes parallel to the substrate, as discussed in the XRD pattern analysis. Besides, it is noted that some bright pillar-like domains are formed in the film. These domains might be formed as a result of the atomic composition variation within the film, i.e., Fe-rich in these "pillars" than the rest part of the film, thus form the nanopillar-like Fe-rich domains. At the meantime, the "matrix" is Mn-rich. As Fe has smaller atomic number than Mo, the Fe-rich regions show brighter contrast in the TEM mode. Fig. 2(b) shows the corresponding SAED pattern taken along the [100] zone axis. Distinguished diffraction dots in the SAED pattern indicate the highly epitaxial growth of the BMoFeO SC structure and confirm the (00*l*) growth direction of the layered thin films. Fig. 2(c) shows the scanning transmittance electron microscopy (STEM) image of the BMoFeO film taken under the high angle annular dark field (HAADF) mode of the same area which shows clear SC structure with the same domain structure but with inverted contrast. STEM under HAADF mode is also called Z-contrast and the image contrast is proportional to Z^2. The Fe-rich and Mo-rich domains are marked by the yellow and purple arrows, respectively. Fig.

2(d) shows the HRSTEM image of the sample taken at the domain boundary area, where the black dash line represents the boundary between the Fe-rich domain (dark contrast due to lower atomic number) and Mo-rich domain (brighter contrast due to higher atomic number). The film shows an obvious Aurivillius structure with alternatively aligned Bi-O layers and Mo/M_T-O layer, as shown in Fig. 1(a). It is interesting to note that the horizontal SC layers are continuous throughout the domain boundaries, which proves the domains in the BMoFeO thin film are caused by the compositional differences, instead of crystal structure difference. Fig. S2 shows the fast-Fourier transform (FFT) filtered image obtained from the selected area in HRSTEM image, where there is no dislocation observed at the grain boundary, which again demonstrates the continuity of the SC structure across the domain boundaries. This observed phenomenon explains why there is no secondary phase peak in the XRD pattern shown in Fig. 1(b). Similar results have been observed in the films with other compositions, such as Bi_3MoMnO_9 (BMoMnO), Bi_3MoCoO_9 (BMoCoO) and Bi_3MoNiO_9 (BMoNiO), as shown in Fig. S3. Fig. 2(e) shows the corresponding cross-sectional EDS mapping of the BMoFeO thin film, where the Fe and Mo elements are marked in yellow and purple, respectively. This image shows clear Fe-rich pillar-like domains embedded in the Mo rich matrix. An EDS line scan at the green arrow marked region in Fig. 2(f) shows the Fe and Mo distribution, marked in yellow and purple, respectively. Both elements exist in the entire scanned region, while the Fe shows an obvious composition jump in the pillar area, which confirms the Fe-rich pillar area. The atomic fraction of Mo is higher in the Mo-rich matrix area than that in the pillars. This result confirms that the domains in the BMoFeO thin film are formed by the distribution of Fe and Mo atoms. In $BMoM_TO$ thin films, the Mo and M_T atoms in the Mo/M_T layers occupy the equivalent position within the unit cells, while the atomic ratios of the Mo and M_T atoms vary in different regions. This variation generates different domains shown in EDS

mappings, but the layered structure is maintained across the domain boundaries. As the cross-sectional EDS only shows very localized information and the EDS composition is for estimation, the sum of the Mo and Fe atomic ratio varies slightly across the green arrow. Besides, the dark and bright contrast areas observed in the TEM and STEM images might be due to the local non-uniform elemental distribution and the non-uniformity is minor, which is originated from the TEM sample preparation.

Piezoresponse force microscopy (PFM) measurements were performed to explore the electric properties of the $BMoM_TO$ thin films, as shown in Fig. 3. $SrRuO_3$ (SRO) buffer layers were grown first as the bottom electrodes. The left panel of each figure show the phase (plotted in blue) and amplitude (plotted in red) switching curves of the $BMoM_TO$ with different M_T elements (Mn, Fe, Co and Ni, respectively). For all four films, the phase curves show obvious hysteresis loops with 180^o phase switching when the bias directions are switched and the amplitude curves show the butterfly-like shape. These curves indicate the ferroelectric nature of the $BMoM_TO$ thin films. The right panels of the figures show the OP phase switching images after a writing and re-writing process, where the positive tip biases were first applied on 0.5 x 0.5 μm^2 areas followed by the negative tip biases applied on 0.2 x 0.2 μm^2 areas. After the writing and re-writing processes, distinct phase switching can be observed, which furtherly confirms the ferroelectric properties in all the $BMoM_TO$ thin films. All above measurements were conducted at 300 K, demonstrating the room temperature ferroelectric nature of the $BMoM_TO$ thin films. It has been previously reported that the ferroelectricity in BMoO thin films are due to the displacement of the Mo cations in the non-central symmetry crystal lattice,[33] therefore the room temperature ferroelectric property of the $BMoM_TO$ thin films might be originated from the displacement of both Mo and M_T cations and non-central symmetry lattice structure.

To explore the magnetic properties of the $BMoM_TO$ thin films, ferromagnetic hysteresis loops were obtained using the magnetic property measurement system (MPMS). Fig. 4(a) and (b) show the room temperature M-H curves of the $BMoM_TO$ thin films with the magnetic fields applied in-plane (IP) and OP, respectively. The insets of the figures illustrate the directions of the applied fields. As shown in the figures, the $BMoM_TO$ thin films show strong ferromagnetic properties at room temperature, in both IP and OP directions. As a comparison, pure BMoO film only shows very weak magnetic response, as plotted in Fig. S4. The huge enhancement of the magnetic response in the $BMoM_TO$ thin films is attributed to the incorporation of the magnetic elements M_T (e.g., Mn, Fe, Co and Ni). Interestingly, the IP anisotropic magnetic property, i.e., stronger magnetic response in the IP direction, has been observed in most of the $BMoM_TO$ thin films, including BMoFeO, BMoMnO and BMoNiO, which is possibly due to the easy IP magnetocrystalline axis for the layered structure, similar to the pure BMoO case. Differently, the BMoCoO sample shows better ferromagnetic response along the OP direction. This might be related to the poorer film quality (as shown in Fig. S3(f)) which results in the OP anisotropy. The ferromagnetic property variation in $BMoM_TO$ films might be resulted from the different dopant elements in the films as well as the change of the domain structure. Overall, the coexistence of ferroelectricity and ferromagnesium under room temperature demonstrates the room temperature multiferroic properties of all the $BMoM_TO$ thin films.

Tunable optical responses in $BMoM_TO$ thin films are also expected because of the various M_T dopants and the unique nanopillar-in-matrix structures. First, transmittance measurements were conducted. Fig. 4(c) shows the optical transmittance spectra of the $BMoM_TO$ thin films as a function of the wavelength. The corresponding direct band gaps of each film were calculated using the Tauc method, and shown in Fig. 4(d) with an inset showing the enlarged plot labelling the band

gaps of each film. The band gap of the BMoO thin films is estimated to be 2.65 eV, which is comparable to previous reported values.[34–36] By changing magnetic elements M_T in the system, tunable direct band gaps of the $BMoM_TO$ thin films arranging from 2.44 eV to 2.82 eV were obtained for Mn, Co, pure, Fe, and Ni. This tuning result might be attributed to the minor structural change based on the ionic size reduction of M_T ions in the lattice, as well as the shape, size and density of the pillar domains. The angular dependence of the transmittance spectra has been studied and is shown in Fig. S5. It can be observed that the on-set points (marked by the arrows) shift to the left as the incident beam angle increases. The shift of the on-set points versus the incident beam angles suggests the anisotropic nature of the optical properties in the BMM_TO thin films, which is originated from the layered structure of the Aurivillius phase thin films.[14] The peaks observed at around 480 nm are the errors caused by the detector.

The ellipsometry experiments were conducted to further explore the anisotropic optical properties of the $BMoM_TO$ thin films. Fig. 5(a-e) shows the fitted real dielectric constants of the thin films in both IP ($\varepsilon_{//}$ marked with dashed lines) and OP ($\varepsilon_{\perp}$ marked with solid lines) directions. It can be seen that the IP dielectric constants of the $BMoM_TO$ thin films have the similar values and trend comparing to the pure BMoO thin film, while the OP dielectric constants vary drastically with the film compositions. All the OP dielectric constants were plotted in Fig. 5(f) for better comparison. More specifically, the OP dielectric constant ($\varepsilon_{\perp}$) decreases from Co, Mn, Fe, pure BMoO, to Ni. This leads to OP anisotropy in Co and Mn cases and IP anisotropy in pure BMoO, Fe and Ni cases. The tunable optical dielectric properties are resulted from the structures. For IP, the layered structure dominates the electronic density of states and the light-matter interactions IP and thus results in the very similar IP ($\varepsilon_{//}$) constant. For OP, depending on the secondary dopants and the structural variation, the density of states in the samples varies and thus results in the largely

different OP dielectric constant ($\varepsilon_{\perp}$). The results of the ellipsometry experiments have demonstrated the tunable optical properties such as OP dielectric constant and overall optical dielectric anisotropy properties. Due to the equipment limitation, the dielectric constants at the bandgap regimes were noisy and thus excluded from the figures.

In this work, the design and fabrication of new nanocomposites by combining an Aurivillius phase material with a perovskite-type transition metal oxide in a unique nanopillar-in-matrix form provide an effective approach of exploring new material systems using layered SC structures. The advantages of the compositional varied domains, instead of the completely different secondary phases, include that (1) high quality layered nanocomposite structures were maintained without much film quality deterioration due to secondary phase growth; (2) novel layered oxide properties remain dominant in IP , such as ferroelectric properties and nonlinearity, while the OP properties are tunable depending on secondary dopant in the systems; (3) highly anisotropic physical properties can be achieved easily in these layered nanocomposite systems by proper selection of the secondary phases, which provides large flexibility in nanocomposite designs and property tuning.

Conclusions

$Bi_3MoM_TO_9$ ($BMoM_TO$, M_T = Mn, Fe, Co and Ni), a new oxide nanocomposite system with SC layered structure as the matrix has been grown on the LAO (001) substrates by the pulsed laser deposition (PLD) technique. The thin films have the pillar-like domains (M_T-rich) embedded in the matrix (Mo-rich). Instead of forming dislocations and other interfacial defects, the atomic lattices are continuous across the domain boundaries. Room temperature multiferroic properties (i.e. ferroelectricity and ferromagnetism) have been demonstrated in the new systems. Anisotropic multifunctionalities, including ferromagnetism, optical transmittance and dielectric anisotropy,

have been demonstrated as a function of the secondary phase composition M_T. As the film composition (i.e. M_T) varies, the magnetic anisotropy, optical bandgap, dielectric function can be effectively tuned. These tunable multifunctionalities in these layered oxide nanocomposite systems present promising applications toward sensors, data storage, high-temperature electronics, memory devices and non-linear optical devices.

Experimental Section

The $BMoM_TO$ targets as well as a pure BMoO target were prepared by conventional solid-state sintering methods. The thin films were deposited onto single crystal $LaAlO_3$ (LAO) (001) substrates using pulsed laser deposition (PLD, KrF, λ = 248 nm) with an optimized substrate temperature of 600 ^oC and oxygen pressure of 200 mTorr during the thin film growth. After the deposition, the as-deposited samples were cooled down to 400 ^oC with a rate of 5 ^oC/min at a 500 Torr oxygen atmosphere and subsequently annealed for one hour to reduce the oxygen vacancies. $SrRuO_3$ (SRO) buffer layers were firstly deposited onto the substrates as bottom electrodes for ferroelectric measurements. The microstructure of fabricated thin films were investigated by X-ray diffraction (XRD, PANalytical Empyrean) and transmittance electron microscopy (TEM, Thermo Scientific TALOS F200X and Thermo Scientific TEAM 1). The piezoelectric properties were measured by the atomic force microscopy (AFM, Bruker Dimension Icon) and piezoresponse force microscopy (PFM) with a conductive Pt-Ir coated Si tip (SCM-PIT). The magnetic properties were investigated using a magnetic property measurement system (MPMS, Quantum Design MPMS-3) with the magnetic field applied in both in-plane (IP) and out-of-plane (OP) directions. The normal incident depolarized transmittance (T%) of the films were carried using an optical spectrophotometer (Lambda 1050 UV/Vis Spectrophotometer) with a spectrum range of 250-800 nm and incident angle of 15^o, 30^o, 45^o, 60^o and 75^o, respectively. The direct band gaps were

estimated by the Tauc method from the transmittance result obtained at 15^{o}. The ellipsometry experiments were examined on a RC2 spectroscopic ellipsometer (J.A. Woollam Company) with a spectrum range of 1000-2000 nm and three angles of 50^{o}, 60^{o} and 70^{o}. The real dielectric constants of the thin films were then retrieved from the software (CompleteEase, J.A. Woollam Company) using the Spline or Gen-Osc model.

Acknowledgements

The work is supported by the U.S. Office of Naval Research (N00014-16-1-2465) for thin film growth and U.S. National Science Foundation (DMR-1565822) for HR(S)TEM work. J.J., D.Z. acknowledge the partial support from the U.S. Office of Naval Research (N00014-20-1-2043). Z. H. acknowledges the support from the U.S. National Science Foundation (DMR-1809520).

References

1. Frit, B. & Mercurio, J. P. The crystal chemistry and dielectric properties of the Aurivillius family of complex bismuth oxides with perovskite-like layered structures. *J. Alloys Compd.* **188**, 27–35 (1992).

2. Zhang, L., Wang, W., Shang, M., Sun, S. & Xu, J. Bi_2WO_6@carbon/Fe_3O_4 microspheres: Preparation , growth mechanism and application in water treatment. *J. Hazard. Mater.* **172**, 1193–1197 (2009).

3. Yan, H. *et al.* The effect of (Li, Ce) and (K, Ce) doping in Aurivillius phase material $CaBi_4Ti_4O_{15}$. *Mater. Res. Bull.* **39**, 1237–1246 (2004).

4. Du, H. & Shi, X. Dielectric and piezoelectric properties of barium-modified Aurivillius-type $Na_{0.5}Bi_{4.5}Ti_4O_{15}$. *J. Phys. Chem. Solids* **72**, 1279–1283 (2011).

5. Jardiel, T., Caballero, A. C. & Villegas, M. Aurivillius ceramics: $Bi_4Ti_3O_{12}$-based piezoelectrics. *J. Ceram. Soc. Japan* **116**, 511–518 (2008).

6. Spectroscopy, P. A transmission electron microscope and group theoretical study of the new Bi-based high-T_c superconductors and some closely related Aurivillius phases. *J. Phys. C Solid State Phys.* **21**, 6067–6083 (1988).

7. Liang, J. K. *et al.* Crystal Structure and Superconductivity of $Bi_2Sr_2CaCu_2O_8$ Compound. *Mod. Phys. Lett. B* **2**, 483–489 (1988).

8. Yee, K. A., Albright, T. A., Jung, D. & Whangbo, M. Aurivillius Phases : A Possible New Class of Metal Oxide Superconductors. *Angew. Chemie Int. Ed.* **28**, 750–751 (1989).

9. Kohri, H., Kato, M., Ohsugi, I. J. & Shiota, I. Thermoelectric Generating Properties of

Perovskite Like Materials. *Adv. Sci. Technol.* **74**, 72–76 (2010).

10. Kohri, H. & Yagasaki, T. Thermoelectric Generating Properties of Aurivillius Compounds. *Adv. Sci. Technol.* **77**, 285–290 (2012).

11. Naresh, G. & Mandal, T. K. Excellent Sun-Light-Driven Photocatalytic Activity by Aurivillius Layered Perovskites, $Bi_{5-x}La_xTi_3FeO_{15}$ (x = 1,2). *ACS Appl. Mater. Interfaces* **6**, 21000–21010 (2014).

12. Muktha, B., Priya, M. H., Madras, G. & Row, T. N. G. Synthesis, Structure, and Photocatalysis in a New Structural Variant of the Aurivillius Phase: $LiBi_4M_3O_{14}$ (M = Nb, Ta). *J. Phys. Chem. B* **109**, 11442–11449 (2005).

13. Kendall, K. R., Navas, C., Thomas, J. K. & Loye, H. Recent Developments in Oxide Ion Conductors : Aurivillius Phases. *Chem. Mater.* **8**, 642–649 (1996).

14. Li, L. *et al.* Novel Layered Supercell Structure from Bi_2AlMnO_6 for Multifunctionalities. *Nano Lett.* **17**, 6575–6582 (2017).

15. Kim, S. & Miyayama, M. Anisotropy in oxide ion conductivity of $Bi_4V_{2-x}Co_xO_{11-\delta}$. *Solid State Ionics* **104**, 295–302 (1997).

16. Yan, H. *et al.* Orientation dependence of dielectric and relaxor behaviour in Aurivillius phase $BaBi_2Nb_2O_9$ ceramics prepared by spark plasma sintering. *J. Mater. Sci. Mater. Electron.* **17**, 657–661 (2006).

17. Ahn, Y., Seo, J. D. & Son, J. Y. Ferroelectric domain structures of epitaxial $CaBi_2Nb_2O_9$ thin films on single crystalline Nb doped (100) $SrTiO_3$ substrates. *J. Cryst. Growth* **422**, 20–23 (2015).

18. Long, C., Fan, H., Li, M., Dong, G. & Li, Q. Crystal structure and enhanced electromechanical properties of Aurivillius ferroelectric ceramics , $Bi_4Ti_{3-x}(Mg_{1/3}Nb_{2/3})_xO_{12}$. *Scr. Mater.* **75**, 70–73 (2014).

19. Araujo, C. A.-P. de, Cuchlaro, J. D., McMillan, L. D., Scott, M. C. & Scott, J. F. Fatigue-free ferroelectric capacitors with platinum electrodes. *Lett. to Nat.* **374**, 627–629 (1995).

20. Al-Shareef, H. N., Dimos, D., Boyle, T. J., Warren, W. L. & Tuttle, B. A. Qualitative model for the fatigue-free behavior of $SrBi_2Ta_2O_9$. *Appl. Phys. Lett.* **68**, 690–692 (1996).

21. Park, B. H. *et al.* Lanthanum-substituted bismuth titanate for use in non-volatile memories. *Lett. to Nat.* **401**, 682–684 (1999).

22. Eerenstein, W., Mathur, N. D. & Scott, J. F. Multiferroic and magnetoelectric materials. **442**, 759–766 (2006).

23. Prellier, W., Singh, M. P. & Murugavel, P. The single-phase multiferroic oxides : from bulk to thin film. *J. Phys. Condens. Matter* **17**, 803–832 (2005).

24. Scott, J. F. Data Storage: Multiferroic Memories. *Nat. Mater.* **6**, 256–258 (2007).

25. Ramesh, R. & Spaldin, N. A. Multiferroics: progress and prospects in thin films. *Nat. Mater.* **6**, 21–29 (2007).

26. Zvezdin, A. K., Logginov, A. S., Meshkov, G. A. & Pyatakov, A. P. Multiferroics: Promising Materials for Microelectronics, Spintronics, and Sensor Technique. *Bull. Russ. Acad. Sci. Phys.* **71**, 1561–1562 (2007).

27. Uratani, Y., Shishidou, T. & Oguchi, T. First-Principles Study on the Magnetic Anisotropy in Multiferroic $PbVO_3$ and $BiCoO_3$. *J. Phys. Soc. Japan* **78**, 084709 (2009).

28. Zhai, L. & Wang, H. The magnetic and multiferroic properties in $BiMnO_3$. *J. Magn. Magn. Mater.* **426**, 188–194 (2017).

29. Jeen, H. *et al.* Growth and characterization of multiferroic $BiMnO_3$ thin films. *J. Appl. Phys.* **109**, 074104 (2011).

30. Wang, H. H. *et al.* Two-Phase Room-Temperature Multiferroic Nanocomposite with $BiMnO_3$-Tilted Nanopillars in the $Bi_2W_{1-x}Mn_xO_6$ Matrix. *ACS Appl. Mater. Interfaces* **11**, 26261–26267 (2019).

31. Wang, H. H. *et al.* Multiferroic vertically aligned nanocomposite with $CoFe_2O_4$ nanocones embedded in layered Bi_2WO_6 matrix. *Mater. Res. Lett.* **7**, 418–425 (2019).

32. Gao, X. *et al.* Vertically Aligned Nanocomposite $BaTiO_3$:$YMnO_3$ Thin Films with Room Temperature Multiferroic Properties toward Nanoscale Memory Devices. *ACS Appl. Nano Mater.* **1**, 2509–2514 (2018).

33. Ismailzade, I. H., Aliyev, I. M., Ismailov, R. M., Alekberov, A. I. & Rzayev, D. A. Ferroelectricity in Bi_2MoO_6. *Ferroelectrics* **22**, 853–854 (1979).

34. Zhang, M. *et al.* One-dimensional Bi_2MoO_6/TiO_2 hierarchical heterostructures with enhanced photocatalytic activity. *CrystEngComm* **14**, 605–612 (2012).

35. Umapathy, V., Manikandan, A., Antony, S. A., Ramu, P. & Neeraja, P. Structure, morphology and opto-magnetic properties of Bi_2MoO_6 nano-photocatalyst synthesized by sol−gel method. *Trans. Nonferrous Met. Soc. China* **25**, 3271–3278 (2015).

36. Yin, W., Wang, W. & Sun, S. Photocatalytic degradation of phenol over cage-like Bi_2MoO_6 hollow spheres under visible-light irradiation. *Catal. Commun.* **11**, 647–650

(2010).

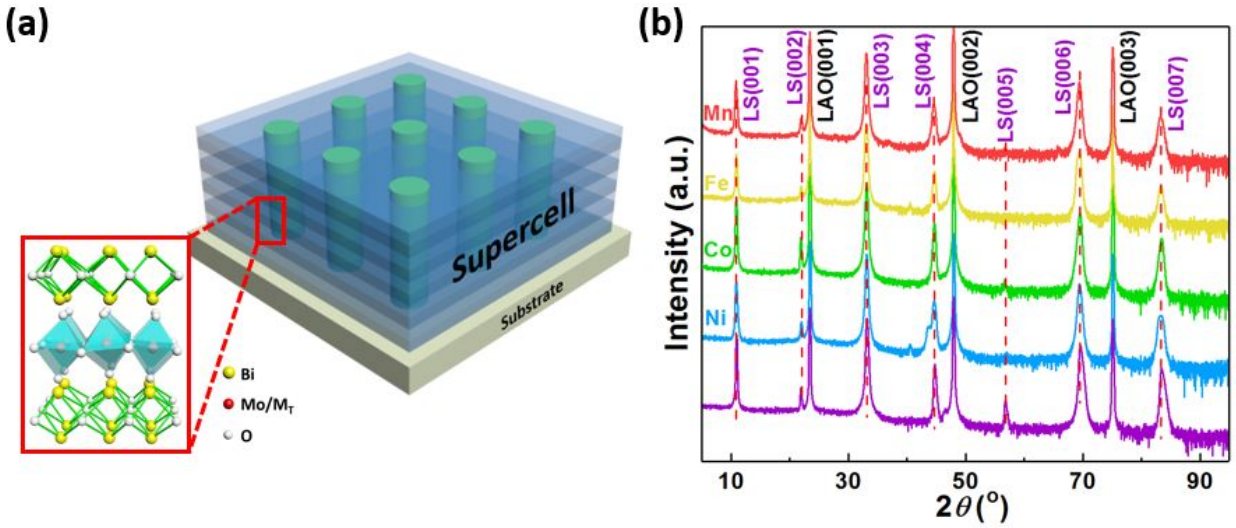

Fig. 1. (a) 3D schematic drawing of the $BMoM_TO$ thin films with pillar like domains embedded in matrix structure. The enlarged schematic illustration demonstrate the film are consist of the alternatively stacked two Bi-O layers and one Mo/M_T-O based layer. (b) θ-2θ XRD scans of $BMoM_TO$ and BMoO thin films. The red dashed lines indicate the positions of the (00*l*) peaks.

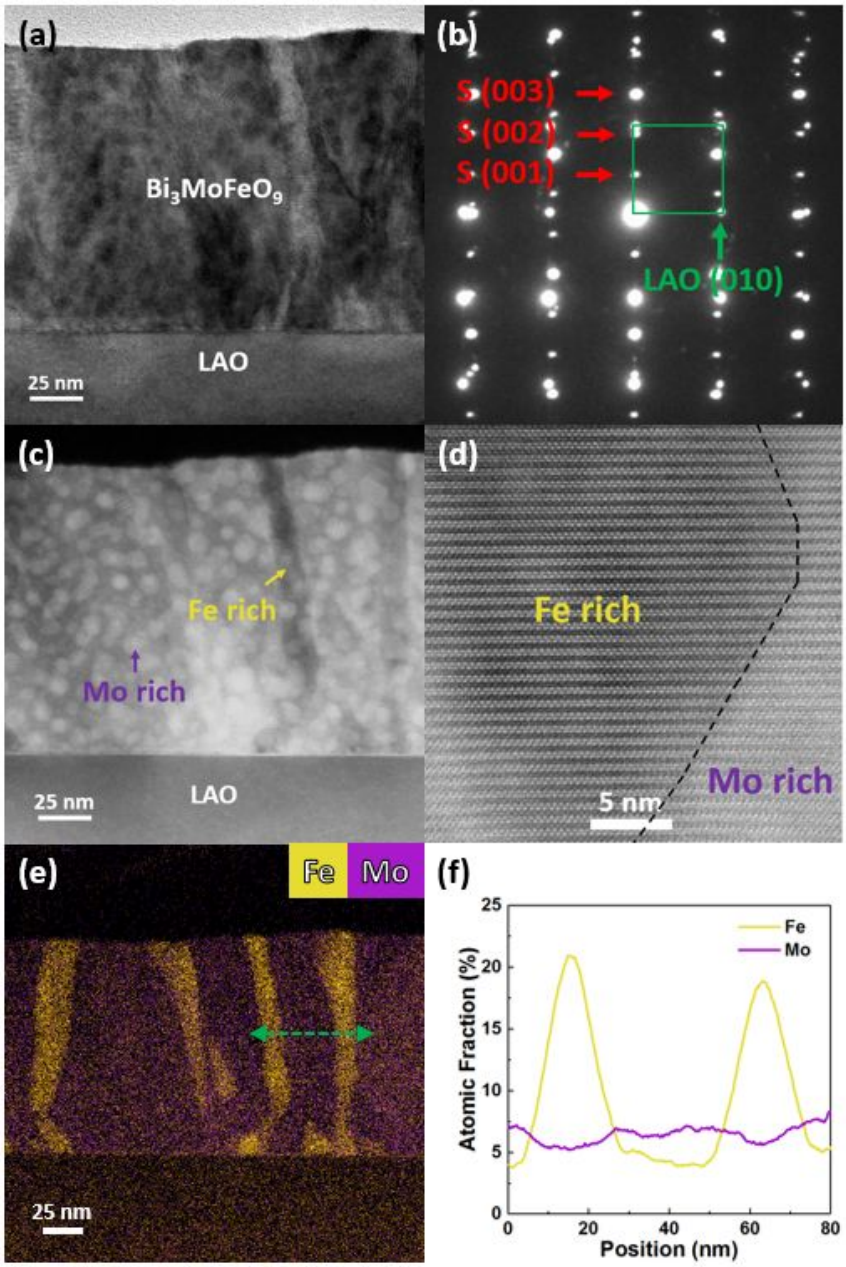

Fig. 2. (a) Cross-sectional TEM image and (b) Selected area electron diffraction (SAED) pattern and (c) STEM image of the BMoFeO thin film. (d) HRTEM image of the BMoFeO thin film, while the black dashed line indicates the domain boundary. (e) Cross-sectional energy-dispersive X-ray spectra (EDS) mapping of Fe (yellow) and Mo (purple) atoms in the BMoFeO film. The green arrow indicates the selected area for: (f) Smoothed linear EDS analysis of the Fe and Mo atoms.

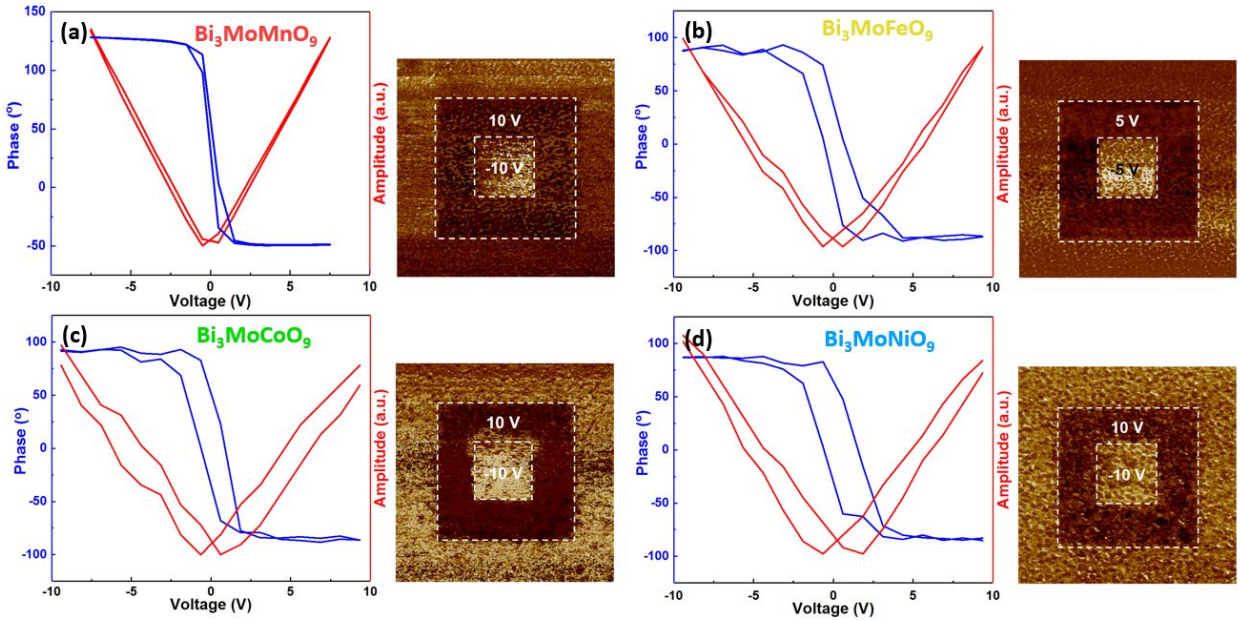

Fig. 3. (a-d) Left panels: the phase (blue) and amplitude (red) switching curves of the $BMoM_TO$ thin films; Right panels: PFM phase image of the $BMoM_TO$ films with different elements (Mn, Fe, Co and Ni, respectively).

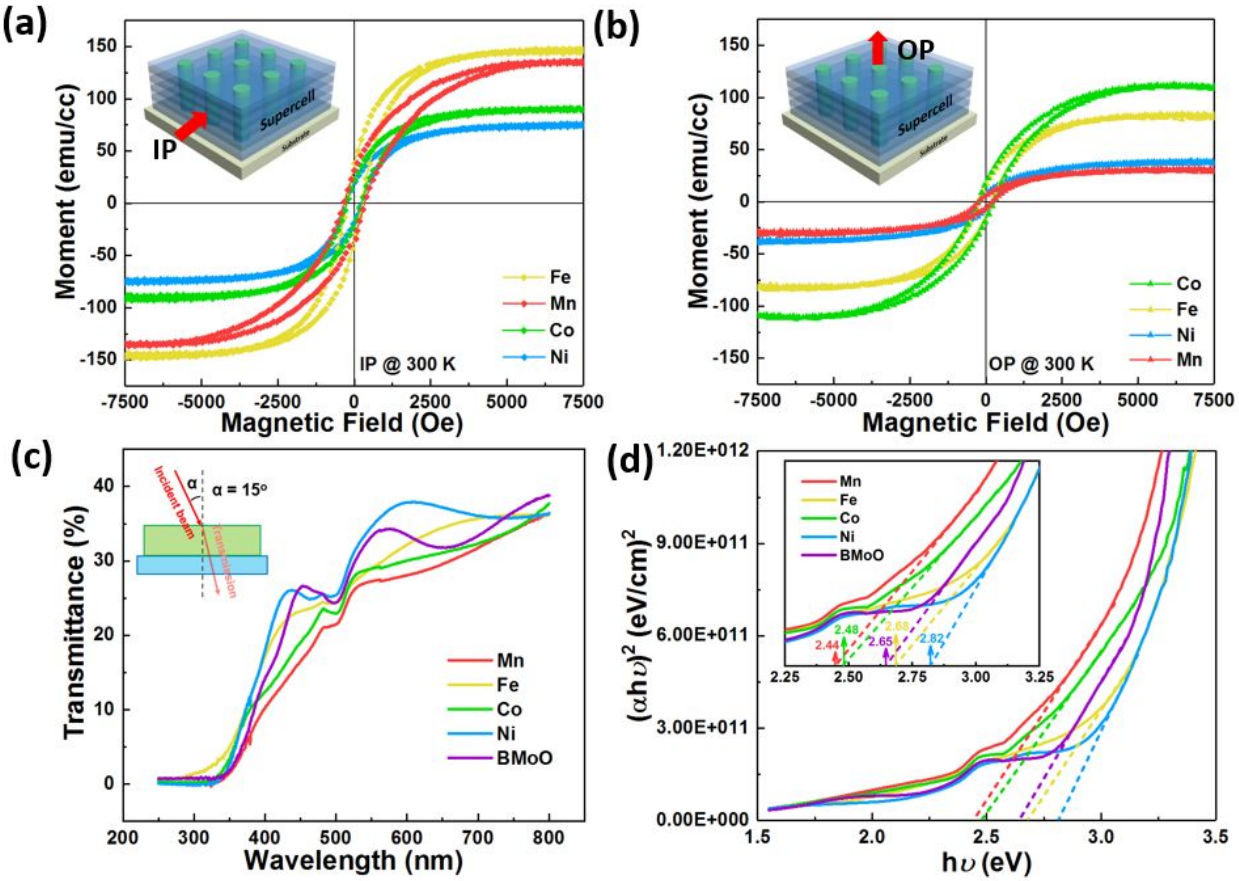

Fig. 4. (a) In-plane and (b) Out-of-plane magnetic hysteresis loops of $BMoM_TO$ films measured at 300 K. The insets show the corresponding magnetic field directions. (c) The optical transmittance spectra of the $BMoM_TO$ thin films as a function of the wavelength, with an incident beam angle of 15°. (d) Direct band gaps of the $BMoM_TO$ and BMoO thin films with the inset showing the enlarged figure and the values of the band gaps.

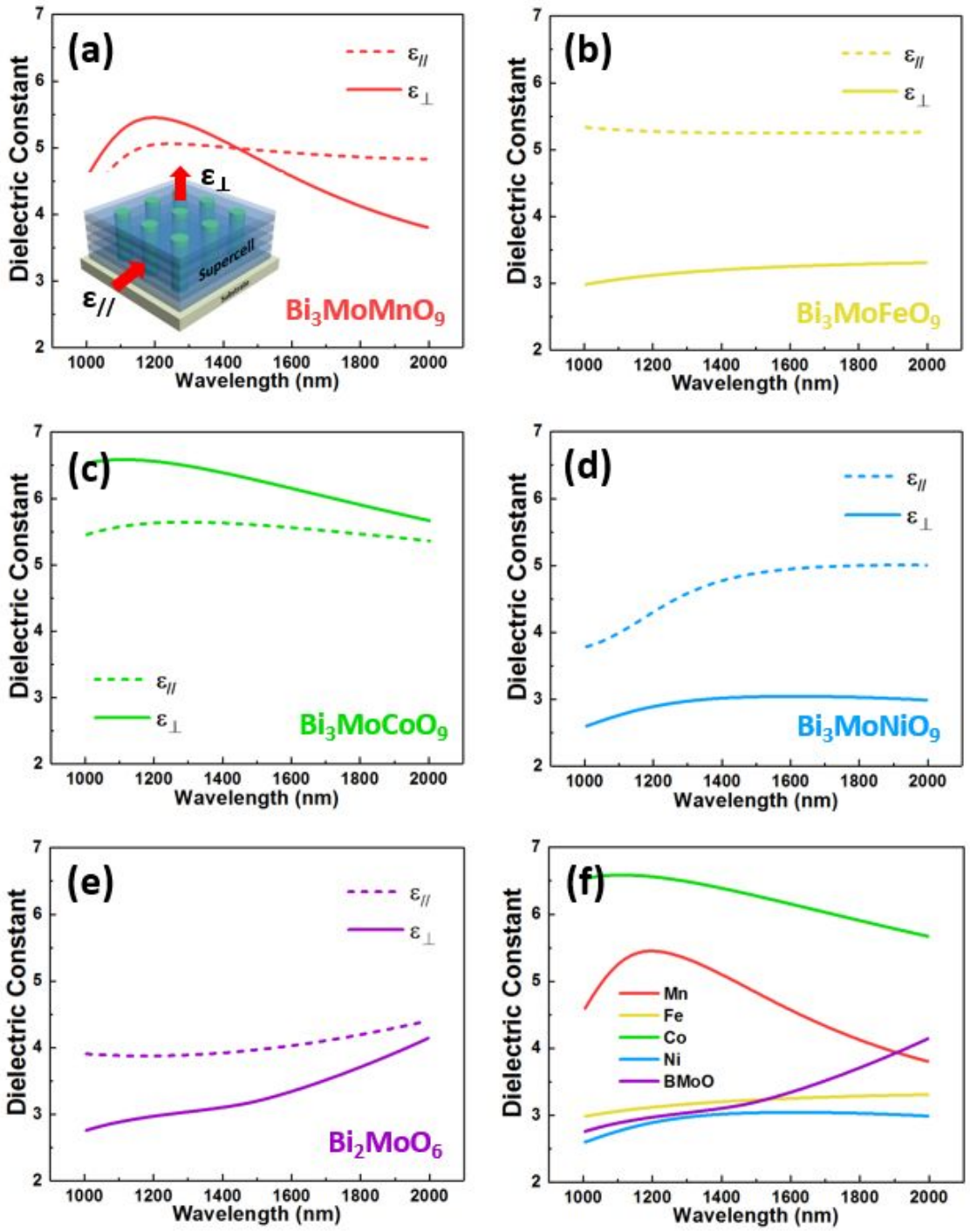

Fig. 5. (a-e) Fitted real dielectric constants of the $BMoM_TO$ and BMoO thin films in both in-plane (marked with dashed lines) and out-of-plane (marked with solid lines) directions. (f) Comparison of the out-of-plane dielectric constants of the $BMoM_TO$ and BMoO thin films.